Lithium-Ion Batteries Hot Paper

Deutsche Ausgabe: DOI: 10.1002/ange.201607951
Internationale Ausgabe: DOI: 10.1002/anie.201607951

A Self-Healing Aqueous Lithium-Ion Battery

Yang Zhao, Ye Zhang, Hao Sun, Xiaoli Dong, Jingyu Cao, Lie Wang, Yifan Xu, Jing Ren, Yunil Hwang, In Hyuk Son, Xianliang Huang, Yonggang Wang, and Huisheng Peng**

Abstract: *Flexible lithium-ion batteries are critical for the next-generation electronics. However, during the practical application, they may break under deformations such as twisting and cutting, causing their failure to work or even serious safety problems. A new family of all-solid-state and flexible aqueous lithium ion batteries that can self-heal after breaking has been created by designing aligned carbon nanotube sheets loaded with $LiMn_2O_4$ and $LiTi_2(PO_4)_3$ nanoparticles on a self-healing polymer substrate as electrodes, and a new kind of lithium sulfate/sodium carboxymethylcellulose serves as both gel electrolyte and separator. The specific capacity, rate capability, and cycling performance can be well maintained after repeated cutting and self-healing. These self-healing batteries are demonstrated to be promising for wearable devices.*

Flexible lithium-ion batteries (LIBs) are critical for the advancement of a variety of fields in which flexible power systems are highly desired, such as portable and wearable electronic devices.[1–5] Although they can normally withstand some deformations such as bending and rolling, they easily break under the complex deformations that often occurs during use, such as twisting. Furthermore, the low thickness of the LIBs, which guarantees a high flexibility, may also lead to complete breakage under accidental cutting. The breakage results in failure of the LIBs or could even cause serious safety problems such as the leakage of toxic electrolyte.[6–9] Therefore, it is highly desired and challenging to rapidly and efficiently solve the breakage problem.

Living organisms can survive mechanical injuries and recover bodily functions owing to the self-healing of the wounds.[10–12] This self-healing functionality greatly increases the survivability of creatures. Inspired by this phenomenon, a series of self-healing polymers have been studied to heal damage based on the reconstruction of the break interface by reversible chemical bonds[13,14] or specific interactions such as ligand–metal bonding,[15] host–guest interaction,[16,17] and hydrogen bonding.[18,19] Recently, several self-healing electronic devices have been fabricated.[20–28] However, LIBs that are capable of self-healing have not been realized owing to the difficulties in designing appropriate electrodes and battery structures to enable efficient self-healing for all the components simultaneously. Additionally, conventional organic electrolytes decompose rapidly in air once the LIBs are damaged,[29,30] which further increases the complexity to achieve the self-healing functionality. It is of both scientific and technological importance to explore this kind of LIB. The self-healing capability of the LIBs will be critical for wearable electronics in the near future.

Herein, a new family of self-healing aqueous LIBs is presented for the first time, to the best of our knowledge, by designing aligned carbon nanotube (CNT) sheets loaded with $LiMn_2O_4$ (LMO) and $LiTi_2(PO_4)_3$ (LTP) nanoparticles on a self-healing polymer substrate as electrodes and aqueous lithium sulfate/sodium carboxymethylcellulose (Li_2SO_4/CMC) as both gel electrolyte and separator. The cooperation of self-healing polymer with the electrical and healing properties of the aligned CNT sheets electrode and Li_2SO_4/CMC gel electrolyte are key to achieve high flexibility and good recovery of electrochemical performance. In particular, the electrochemical storage capability was well maintained after several cutting and self-healing cycles.

The fabrication of the self-healing electrodes is shown in Figure 1 a. A free-standing self-healing polymer substrate (see the photographs and chemical structure in Figures S1–S3 of the Supporting Information) was prepared by a modified Leibler's method.[18] A spinnable CNT array (Supporting Information, Figure S4) was first synthesized by chemical vapor deposition.[31–33] As shown in the Supporting Information, Figure S5, a blade was then on the top top edge of the CNT array to continuously pull out an aligned CNT sheet (Supporting Information, Figure S6). The aligned CNT sheets were flexible with high tensile strengths and electrical conductivities, which made them promising candidates as electrodes for the construction of flexible LIBs.

LMO and LTP nanoparticles served as active materials in aqueous LIBs and were synthesized by solid-phase synthesis[34] and sol-gel methods,[35,36] respectively. The LMO and LTP nanoparticles were uniformly dispersed in the electrodes (Figures 1 b,d) and had diameters of hundreds of nanometers (Supporting Information, Figures S7–S9). The spinel phase of LMO (Supporting Information, Figure S10) and the NASI-

[*] Y. Zhao, Y. Zhang, H. Sun, J. Cao, L. Wang, Y. Xu, J. Ren, Prof. H. Peng
State Key Laboratory of Molecular Engineering of Polymers, Department of Macromolecular Science and Laboratory of Advanced Materials, Fudan University
Shanghai 200438 (China)
E-mail: penghs@fudan.edu.cn

X. Dong, Prof. Y. Wang
Department of Chemistry and Shanghai Key Laboratory of Molecular Catalysis and Innovative Materials, Institute of New Energy, iChEM (Collaborative Innovation Center of Chemistry for Energy Materials), Fudan University
Shanghai 200438 (China)
E-mail: ygwang@fudan.edu.cn

Y. Hwang, Dr. I. H. Son
Energy Materials Lab, Materials Research Center, Samsung Advanced Institute of Technology, Samsung Electronics Co., LTD.
130 Samsung-ro, Suwon-si, Gyeonggi-do 443803 (South Korea)

Dr. X. Huang
Samsung R&D Institute China
Beijing 100028 (China)

Supporting information for this article can be found under: http://dx.doi.org/10.1002/anie.201607951.

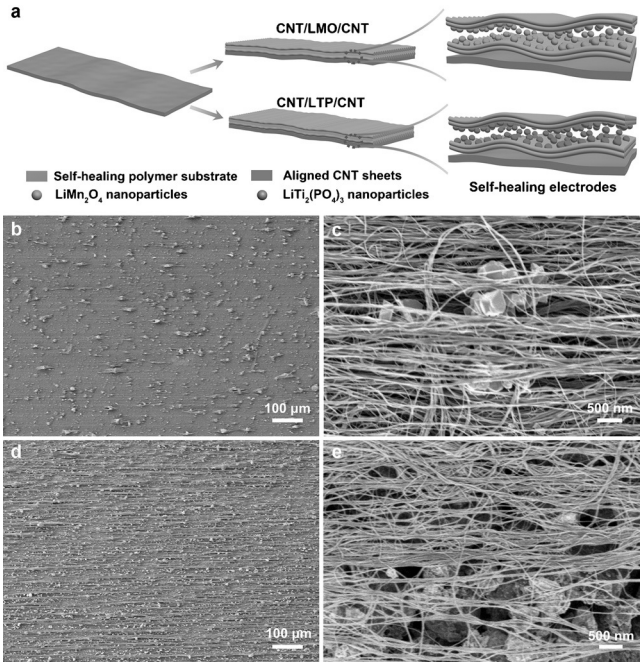

Figure 1. a) Schematic of the fabrication process of the self-healing electrodes. b) and c) SEM images of CNT/LMO/CNT cathode at low and high magnifications, respectively. d) and e) SEM images of CNT/LTP/CNT anode at low and high magnifications, respectively.

CON-type phase of LTP (Supporting Information, Figure S11) were confirmed by X-ray diffraction. The LMO or LTP nanoparticles were dispersed and physically attached onto the aligned CNTs (Supporting Information, Figures S12 and S13). Several aligned CNT sheets were then stacked onto the aligned CNT composite sheets to form the CNT/LMO/CNT or CNT/LTP/CNT film (Figures 1 c,e). Their electrochemical properties were verified by galvanostatic charge–discharge measurements (Supporting Information, Figures S14 and S15) and cyclic voltammetry (Supporting Information, Figures S16 and S17) in Li_2SO_4 solution. The reactions at the cathode and anode are summarized as Eq. (1) and Eq. (2). The balancing mass ratio of cathode and anode was designed to be 1:1 owing to their comparable specific capacities ($mAh\,g^{-1}$). The Supporting Information Figures S18 and S19 show the galvanostatic charge–discharge curves and cyclic performance of the full LIB tested in Li_2SO_4 solution, respectively. Note that the capacities occasionally fluctuated in Figure S19 possibly owing to slight fluctuations of the Li_2SO_4 solution level during the test.

$$\text{Cathode}: \quad LiMn_2O_4 \leftrightarrow Li_{1-x}Mn_2O_4 + x\,Li^+ + x\,e^- \qquad (1)$$

$$\text{Anode}: \quad LiTi_2(PO_4)_3 + 2x\,Li^+ + 2x\,e^- \leftrightarrow Li_{1+2x}Ti_2(PO_4)_3 \qquad (2)$$

The polymer substrates consisted of supramolecular polymer networks that were rich in multiple hydrogen bonds, which can reconstruct after breaking. Differential scanning calorimetry (DSC) curves showed a low glass transition temperature of approximately −15 °C (Supporting Information, Figure S20), which was beneficial for the reconstruction of hydrogen bond networks at room temperature. The Supporting Information Figure S21 shows optical micrographs of the self-healing polymer after cutting and self-healing, and it was almost fully recovered to the initial state after the fractured surfaces were brought into contact. The self-healing polymer demonstrated good mechanical properties to serve as the support substrate for both the CNTs and active particles (Supporting Information, Figure S22). The CNT/LMO/CNT and CNT/LTP/CNT films were then attached onto the self-healing polymer substrate as the effective cathode and anode, respectively.

The self-healing electrodes demonstrated good electrical and mechanical self-healing performance. They were flexible and could be bent or twisted (Supporting Information, Figure S23). The freestanding electrode was able to heal itself after cutting (Figures 2 a–c) and could still be bent or twisted without damage (Supporting Information, Figure S24). Once the electrode was cut, large amount of hydrogen bonds broke. When the two broken parts were brought into contact, the broken hydrogen bond networks were reconstructed at the surfaces of the fracture. The broken aligned CNTs attached onto the substrate were also reconnected (Supporting Information, Figure S25) by Van der Waals forces to recover the electrical conductivity of the electrode (Supporting Information, Figure S26), which was further verified by the optical micrographs (Figures 2 d–f). As shown in the Supporting Information, Figure S27, the electrode could be cut in different directions relative to the alignment of the CNTs. The electrical resistance of the electrodes remained stable after many cutting–healing cycles in all three cutting directions (Figures 2 g and the Supporting

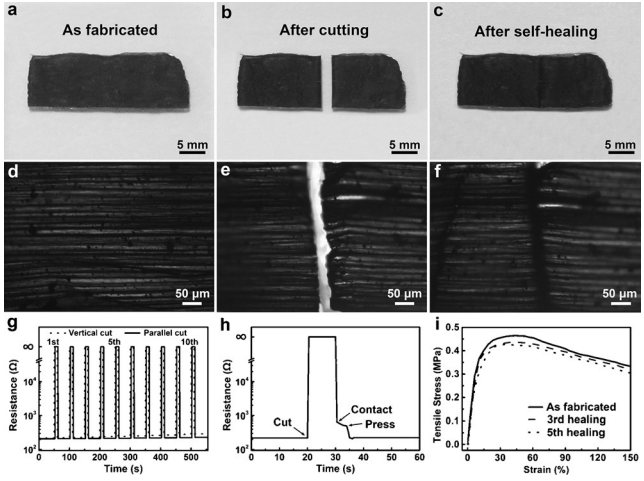

Figure 2. The electrical and mechanical self-healing performance of the self-healing electrodes. a–c) Photographs of the self-healing electrode before breaking, after cutting and self-healing, respectively. d–f) Micrographs of the self-healing electrode before breaking, after cutting, and after self-healing. g) Electrical resistances of the self-healing electrodes over ten cutting–healing cycles under vertical and parallel cutting (relative to the CNT-aligned direction). h) Electrical resistances of the self-healing electrode during a full cutting–healing cycle. i) Stress–strain curves of the self-healing electrode before and after the cutting–healing process.

Information, Figure S28). However, the increase in electrical resistance for the parallel cutting direction was lower than that in the vertical cutting direction. This phenomenon may be explained by the fact that many more CNTs broke under vertically cutting compared with the parallel cutting. Therefore, the electrodes and LIBs were both cut vertically unless otherwise specified.

We also compared the self-healing performance between electrodes made from the aligned CNT composite sheet or randomly dispersed CNT composite film (Supporting Information, Figure S29). Obviously, the aligned CNT composite electrode showed a much higher self-healing performance, which was caused by a better reconnection for the broken aligned CNTs. Therefore, aligned CNT composite electrodes were used to fabricate the self-healing LIBs in the following discussion. During a full cutting–healing cycle, the electrical resistance of the electrode increased slightly by 2.3% after healing (Figure 2h). Figure 2i shows a comparison of the stress–strain curves of the electrode after three and five cutting–healing cycles, with the tensile strengths maintained by 94.0% and 91.8%, respectively.

The self-healing aqueous LIB was finally fabricated by pairing the self-healing cathode and anode with the Li_2SO_4/CMC gel electrolyte between them (Supporting Information, Figure S30). The Li_2SO_4/CMC gel electrolyte was prepared by mixing a physically cross-linked CMC gel and a Li_2SO_4 aqueous solution, exhibiting an ionic conductivity of 0.12 $S\,cm^{-1}$ at 298 K (Supporting Information, Figure S31). The gel electrolyte was in good contact with the electrode (Supporting Information, Figure S32). Compared with the combustible and toxic organic electrolytes, which immediately decompose upon exposure to the air, the aqueous Li_2SO_4 gel electrolyte was safe and nontoxic with a high stability in air.

As shown in Figure 3a, after being cut into two separate parts, the aqueous LIB can be healed to recover the normal functionality by simply bringing into contact the two parts for a few seconds. Before being cut, the aqueous LIB showed a specific capacity of 28.2 $mAh\,g^{-1}$ at a current density of 0.5 $A\,g^{-1}$ (Figure 3b), which was lower than that measured in the Li_2SO_4 solution (Supporting Information, Figure S19) owing to the much lower ionic conductivity and higher interface impedance of the gel electrolyte compared with the aqueous Li_2SO_4 solution. When the current density decreased to 0.1 $A\,g^{-1}$, a higher specific capacity of 44.5 $mAh\,g^{-1}$ was achieved, which was comparable to that measured in the Li_2SO_4 solution. The self-healing properties were then investigated by monitoring the electrochemical properties. Before cutting and after the third self-healing, the discharge voltage plateau slightly decreased from 1.58 to 1.45 V due to the increased electrical resistance of the electrode (Figure 3c). After the fifth self-healing, the specific capacity decreased from 28.2 to 17.2 $mAh\,g^{-1}$ at a current density of 0.5 $A\,g^{-1}$. The aqueous LIBs also showed a good rate capability after the fifth self-healing (Figure 3d).

To further evaluate the cyclic performance before cutting and after self-healing, the aqueous LIBs were operated for 100 charge/discharge cycles (Figure 3e). The specific capacities were maintained at 82.8% and 69.3% for the as-fabricated LIB and the LIB after the fifth healing, respectively, indicating the cycling performance was well maintained after repeated cutting and healing cycles. After the cutting–healing cycles, the mechanical strength of the self-healing LIB was well maintained (Supporting Information, Figure S33). The electrical and mechanical self-healing properties of the LIB were the result of the combined self-healing capabilities of the polymer substrate, aligned CNT sheets and gel electrolyte.

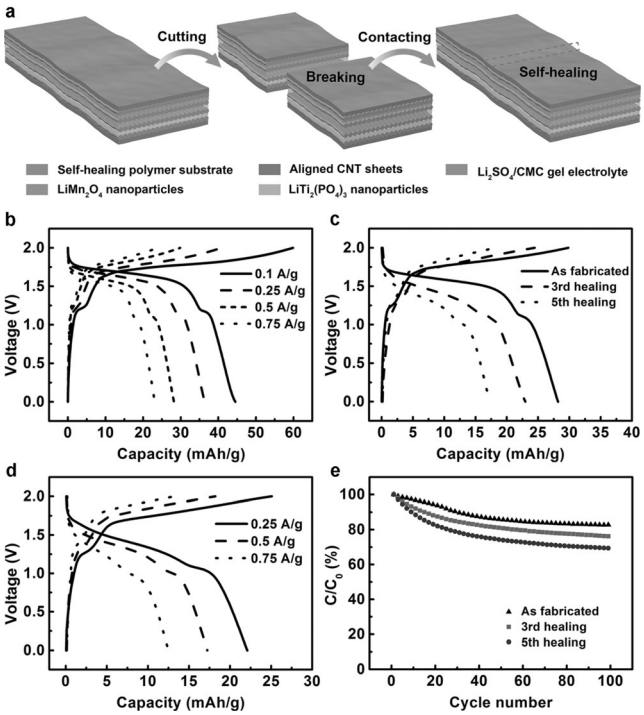

Figure 3. The electrochemical self-healing performance of the self-healing aqueous LIB. a) Schematic of the self-healing process of the LIB. b) Rate capability of the as-fabricated self-healing aqueous LIB. c) Galvanostatic charge–discharge curves of the aqueous LIB after different numbers self-healing cycles at a current density of 0.5 $A\,g^{-1}$. d) Rate capability of the self-healing aqueous LIB after the fifth self-healing. e) Cyclic performance of aqueous LIBs with different numbers of self-healing cycles at a current density of 0.5 $A\,g^{-1}$.

These self-healing aqueous LIBs also demonstrated high flexibility. There were no obvious changes in the charge and discharge profiles before and after bending at 30° and 60° (Figure 4a). After 200 bending cycles at 60°, the specific capacity was maintained by 90.3% (Figure 4b). As an application demonstration, a self-healing LIB was placed around the elbow of a puppet to power a red light-emitting diode (LED) (Figure 4c). When the self-healing LIB was completely cut through, the LED lamp went out immediately (Figure 4d). Upon carefully bringing the two broken parts into contact for a few seconds, the red LED lit up again without obvious change in the brightness (Figure 4e), showing good healing efficiency of the aqueous LIB. No safety hazard was observed when the self-healing LIB was drilled through during use (Supporting Information, Figure S34). Therefore, this self-healing aqueous LIB can rapidly and efficiently solve the breaking problem during the practical use.

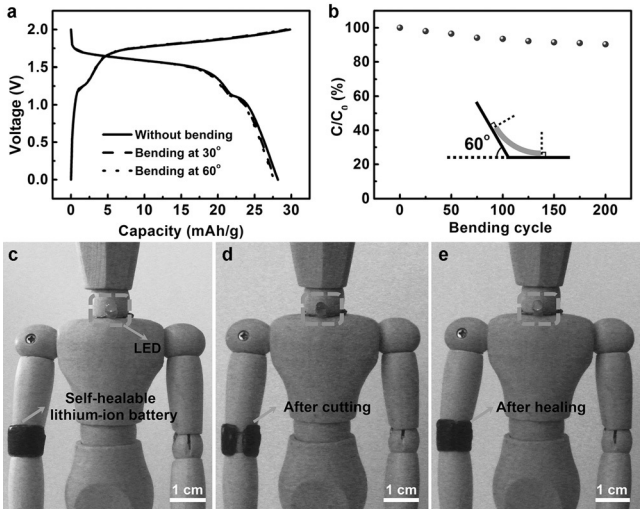

Figure 4. a) Galvanostatic charge–discharge curves of the self-healing aqueous LIB bent to different angles at a current density of 0.5 $A g^{-1}$. b) The capacity retention of the self-healing aqueous LIB with increasing bending cycles at a bending angle of 60°. C_0 and C correspond to the specific capacity before and after bending, respectively. c–e) Photographs of the self-healing aqueous LIB placed around the elbow of a puppet. The LIB is shown powering a red LED lamp before cutting (c), after cutting, (d) and after self-healing (e).

The self-healing aqueous LIB realized in this work is of both scientific and technological importance. First, a new kind of self-healing energy storage device based on Li^+ insertion/extraction was developed, which is fundamentally different from the previously reported self-healing energy storage devices. It demonstrated high energy density of 32.04 $Wh kg^{-1}$, which is five-fold higher than the reported highest value, and comparable power density among the reported self-healing energy storage devices (Supporting Information, Figures S35 and S36). Second, the aligned CNT sheets demonstrated a better self-healing performance compared with random CNTs owing to the good alignment. Third, the sandwiched structure of CNT/LMO/CNT and CNT/LTP/CNT hybrid films endowed the electrodes with high mechanical strength and flexibility, which effectively prevented the peeling off of the active nanoparticles. Finally, the non-toxic aqueous electrolyte developed in this work demonstrated higher safety, stability, and reliability than organic electrolytes, which is promising for wearable applications in the near future.

Acknowledgements

This work was supported by NSFC (21225417, 51573027, 51403038), STCSM (15XD1500400, 15JC1490200) and the Program for Outstanding Young Scholars from the Organization Department of the CPC Central Committee. This work was supported in part by the Samsung Advanced Institute of Technology (SAIT)'s Global Research Outreach (GRO) Program (IO140919-02248-01).

Keywords: carbon nanotubes · flexible electronics · lithium-ion batteries · nanotechnology · self-healing polymers

How to cite: *Angew. Chem. Int. Ed.* **2016**, *55*, 14384–14388
Angew. Chem. **2016**, *128*, 14596–14600

[1] H. Nishide, K. Oyaizu, *Science* **2008**, *319*, 737–738.
[2] L. Hu, H. Wu, F. La Mantia, Y. Yang, Y. Cui, *ACS Nano* **2010**, *4*, 5843–5848.
[3] S. Xu, Y. Zhang, J. Cho, J. Lee, X. Huang, L. Jia, J. A. Fan, Y. Su, J. Su, H. Zhang, *Nat. Commun.* **2013**, *4*, 1543.
[4] L. Zhi, D. Kong, Y. Zhang, X. Li, X. Hai, B. Wang, X. Qiu, Q. Yang, *Energy Environ. Sci.* **2016**, *9*, 906–911.
[5] G. Zhou, F. Li, H. M. Cheng, *Energy Environ. Sci.* **2014**, *7*, 1307–1338.
[6] Y. Wang, W. D. Richards, S. P. Ong, L. J. Miara, J. C. Kim, Y. Mo, G. Ceder, *Nat. Mater.* **2015**, *14*, 1026–1031.
[7] E. H. Kil, K. H. Choi, H. J. Ha, S. Xu, J. A. Rogers, M. R. Kim, Y. G. Lee, K. M. Kim, K. Y. Cho, S. Y. Lee, *Adv. Mater.* **2013**, *25*, 1395–1400.
[8] Y. J. Nam, S. J. Cho, D. Y. Oh, J. M. Lim, S. Y. Kim, J. H. Song, Y. G. Lee, S. Y. Lee, Y. S. Jung, *Nano Lett.* **2015**, *15*, 3317–3323.
[9] D. Zhou, Y. B. He, R. Liu, M. Liu, H. Du, B. Li, Q. Cai, Q. H. Yang, F. Kang, *Adv. Energy Mater.* **2015**, *5*, 1500353.
[10] Y. Fuchs, S. Brown, T. Gorenc, J. Rodriguez, E. Fuchs, H. Steller, *Science* **2013**, *341*, 286–289.
[11] R. R. Driskell, B. M. Lichtenberger, E. Hoste, K. Kretzschmar, B. D. Simons, M. Charalambous, S. R. Ferron, Y. Herault, G. Pavlovic, A. C. Ferguson-Smith, *Nature* **2013**, *504*, 277–281.
[12] W. C. Chou, M. Takeo, P. Rabbani, H. Hu, W. Lee, Y. R. Chung, J. Carucci, P. Overbeek, M. Ito, *Nat. Med.* **2013**, *19*, 924–929.
[13] K. Imato, M. Nishihara, T. Kanehara, Y. Amamoto, A. Takahara, H. Otsuka, *Angew. Chem. Int. Ed.* **2012**, *51*, 1138–1142; *Angew. Chem.* **2012**, *124*, 1164–1168.
[14] H. Ying, Y. Zhang, J. Cheng, *Nat. Commun.* **2014**, *5*, 3218.
[15] C. H. Li, C. Wang, C. Keplinger, J. L. Zuo, L. Jin, Y. Sun, P. Zheng, Y. Cao, F. Lissel, C. Linder, X. Z. You, Z. N. Bao, *Nat. Chem.* **2016**, *8*, 618–624.
[16] T. Kakuta, Y. Takashima, M. Nakahata, M. Otsubo, H. Yamaguchi, A. Harada, *Adv. Mater.* **2013**, *25*, 2758–2758.
[17] H. Chen, X. Ma, S. Wu, H. Tian, *Angew. Chem. Int. Ed.* **2014**, *53*, 14149–14152; *Angew. Chem.* **2014**, *126*, 14373–14376.
[18] P. Cordier, F. Tournilhac, C. Soulié-Ziakovic, L. Leibler, *Nature* **2008**, *451*, 977–980.
[19] C. Wang, N. Liu, R. Allen, J. B. H. Tok, Y. Wu, F. Zhang, Y. Chen, Z. Bao, *Adv. Mater.* **2013**, *25*, 5785–5790.
[20] T. P. Huynh, H. Haick, *Adv. Mater.* **2016**, *28*, 138–143.
[21] E. Borré, J. F. Stumbé, S. Bellemin-Laponnaz, M. Mauro, *Angew. Chem. Int. Ed.* **2016**, *55*, 1313–1317; *Angew. Chem.* **2016**, *128*, 1335–1339.
[22] B. C. Tee, C. Wang, R. Allen, Z. Bao, *Nat. Nanotechnol.* **2012**, *7*, 825–832.
[23] H. Sun, X. You, Y. Jiang, G. Guan, X. Fang, J. Deng, P. Chen, Y. Luo, H. Peng, *Angew. Chem. Int. Ed.* **2014**, *53*, 9526–9531; *Angew. Chem.* **2014**, *126*, 9680–9685.
[24] H. Wang, B. Zhu, W. Jiang, Y. Yang, W. R. Leow, H. Wang, X. Chen, *Adv. Mater.* **2014**, *26*, 3638–3643.
[25] C. Wang, H. Wu, Z. Chen, M. T. McDowell, Y. Cui, Z. Bao, *Nat. Chem.* **2013**, *5*, 1042–1048.
[26] Y. Huang, Y. Huang, M. Zhu, W. Meng, Z. Pei, C. Liu, H. Hu, C. Zhi, *ACS nano* **2015**, *9*, 6242–6251.
[27] T. Trivedi, D. Bhattacharjya, J. Yu, A. Kumar, *ChemSusChem* **2015**, *8*, 3294–3303.
[28] Y. Zhao, J. Wei, H. Li, Y. Yan, W. Zhou, D. Yu, Q. Zhao, *Nat. Commun.* **2016**, DOI: 10.1038/ncomms10228.
[29] L. Smith, B. Dunn, *Science* **2015**, *350*, 918–918.

[30] K. H. Park, D. Y. Oh, Y. E. Choi, Y. J. Nam, L. Han, J. Y. Kim, H. Xin, F. Lin, S. M. Oh, Y. S. Jung, *Adv. Mater.* **2016**, *28*, 1874 – 1883.
[31] M. Zhang, K. R. Atkinson, R. H. Baughman, *Science* **2004**, *306*, 1358 – 1361.
[32] H. Peng, X. Sun, F. Cai, X. Chen, Y. Zhu, G. Liao, D. Chen, Q. Li, Y. Lu, Y. Zhu, *Nat. Nanotechnol.* **2009**, *4*, 738 – 741.
[33] L. Qiu, S. He, J. Yang, J. Deng, H. Peng, *Small* **2016**, *12*, 2419 – 2424.
[34] Y. Y. Liang, S. J. Bao, B. L. He, W. J. Zhou, H. L. Li, *J. Electrochem. Soc.* **2005**, *152*, A2030 – A2034.
[35] L. Chen, J. Liu, Z. Guo, Y. Wang, C. Wang, Y. Xia, *J. Electrochem. Soc.* **2016**, *163*, A904 – A910.
[36] J. Luo, Y. Xia, *Adv. Funct. Mater.* **2007**, *17*, 3877 – 3884.

Received: August 15, 2016
Published online: October 12, 2016

